Σ photoproduction in the resonance region

S. Janssen,* J. Ryckebusch, D. Debruyne, and T. Van Cauteren
Department of Subatomic and Radiation Physics, Ghent University, Proeftuinstraat 86, B-9000 Gent, Belgium
(Received 25 February 2002; published 26 September 2002)

A study of $\gamma p \to K\Sigma$ processes in an isobar model at tree level is reported. By comparing model calculations to the published SAPHIR data, we explore the possible role of different isospin $I=\frac{1}{2}$ (N^*) and $I=\frac{3}{2}$ (Δ^*) resonances in the reaction dynamics. In our analysis, the inclusion of the ''missing'' $D_{13}(1895)$ resonance does only slightly improve the global description of the Σ photoproduction data. More convincing signals for the presence of such a ''missing'' resonance emerged in the analysis of the isospin related $\gamma p \to K^+\Lambda$ reaction. Various implementations of the nonresonant part of the Σ photoproduction amplitude are presented. The sensitivity of the computed observables and extracted resonance parameters to the uncertainties inherent to the treatment of the nonresonant (background) diagrams are discussed.

DOI: 10.1103/PhysRevC.66.035202 PACS number(s): 13.30.Eg, 13.60.Le, 14.20.Gk, 25.20.Lj

I. INTRODUCTION

Traditionally, pion photoproduction reactions $\gamma p \to \pi N$ have played a crucial role in studies that aim at elucidating the excitation spectrum of baryons. The study of the far weaker kaon photoproduction channels is currently gaining momentum, thanks to the construction of a number of dedicated photon and electron accelerator facilities in the few GeV photon and electron energy regime. It is believed that the involvement of a $s\bar{s}$ quark antiquark pair in the reaction process opens a new window on the dynamics of excited nucleon states and can help in shedding light on the complex and not so well understood field of baryon spectroscopy. Recently, accurate measurements for the three reactions $\gamma p \to K^+\Lambda$, $\gamma p \to K^+\Sigma^0$, and $\gamma p \to K^0\Sigma^+$ have been reported [1,2]. In the baryon resonance region, the observed total cross sections for all three channels are of the order of a few microbarns.

A property which is specifically related to the production of Σ hyperons, is the anticipated role of the isospin $I=\frac{3}{2}$ Δ^* resonances in the reaction dynamics, which are excluded from participating in Λ photoproduction because of arguments based on isospin conservation. As such, the $\gamma p \to K\Sigma$ channel can act as an isospin filter to study those Δ^* resonances. In comparison to the $\gamma p \to K\Lambda$ process, the description of Σ photoproduction within the context of isobar models appears less attractive, as the freedom to excite Δ^* states increases the number of candidates, and correspondingly the number of parameters, for intermediate resonant states. An important feature which helps in minimizing the number of free parameters, though, is the observation that the Σ^0 and Σ^+ particles are part of the Σ isospin triplet. Consequently, one can rely on isospin symmetry to relate the coupling constants needed in the description of the $p(\gamma,K^+)\Sigma^0$ reaction to those required for the $p(\gamma,K^0)\Sigma^+$ process. Within such a scheme, a common analysis of both reaction channels becomes possible.

In this work, we aim at studying Σ photoproduction at the so-called ''tree level,'' where only first-order Feynman graphs are taken into account. This implies that all higher-order terms, which, for example, account for final-state interaction effects, are being discarded. Also the unitarity constraint is not fully obeyed at tree level. A recent coupled-channel analysis [3], specifically designed to include coupled-channel effects in the description of strangeness photoproduction channels, reports that the effect of coupled-channel mechanisms on the cross sections is of the order of 20%. Admittedly, this is a substantial effect. On the other hand, in the tree-level analysis presented here, we observe substantial model dependences. They give rise to substantial variations in some of the extracted coupling constants. The major source of the model uncertainties stems from the treatment of the background or nonresonant Feynman diagrams. In the light of this, we reckon that a profound understanding of the tree-level contributions to hyperon photoproduction processes is imperative. We are convinced that full-blown coupled-channel analyses will also benefit from an improved understanding of the tree-level contributions to the strangeness photoproduction reactions.

In this work, we extend our tree-level analysis of the Λ photoproduction data reported in Ref. [4] to the Σ channel. The organization of this paper is as follows. In Sec. II, we will discuss the isobar model for hyperon photoproduction on the nucleon. Special attention will be paid to the peculiar role played by the Born diagrams. In Sec. III we then present the results of our numerical calculations. In Sec. III A, we explore the dominant resonance contributions and in Sec. III B we investigate various schemes to implement the nonresonant background terms. In Sec. III C, we discuss in how far the crossing symmetric $K^-p \to \gamma\Sigma^0$ process provides additional constraints for the description of the Σ photoproduction reaction. Section IV contains our conclusions and an outlook. The Appendix summarizes the use of isospin constraints in relating hadronic and electromagnetic coupling constants.

II. ISOBAR MODEL

A. Formalism

In this work, the Σ photoproduction reaction on the proton is modeled with the aid of effective Lagrangians. In such

*Electronic address: stijn.janssen@rug.ac.be

a framework, the physical degrees of freedom are hadrons and their excited states. Every resonance is treated as an individual particle with its own properties, such as mass, strong-decay widths, and photohelicity amplitudes. When calculating the leading Feynman diagrams, effective-field theories provide the operatorial structure of the interaction vertices and the propagators for the intermediate particles. The detailed forms of the effective Lagrangians for the various couplings can be found in many works (see, for example, Refs. [5,6]). The conventions used here are summarized in Ref. [4].

Since the Lagrangian formalism describes point-like interactions, it is a common procedure to introduce phenomenological form factors at the hadronic vertices. They do account for the finite extension of the interacting hadrons and the hard (unknown) physics at short interbaryon distances. We wish to stress that such a phenomenological treatment of the short-distance physics is necessarily model dependent. A widely used parameterization for the hadronic form factors is the dipole form [7]:

$$F_x(\Lambda)=\frac{\Lambda^4}{\Lambda^4+(x-M_x^2)^2} \quad (x\equiv s,t,u), \tag{1}$$

where x is the off-shell momentum squared at the vertex and Λ is the cutoff mass that sets the short-distance scale of the effective theory. It is well known that introducing hadronic form factors violates gauge invariance at the level of the Born diagrams. Additional contact terms are then required to restore this fundamental symmetry, a procedure which is not free of ambiguities. In our calculations, the gauge-restoring contact terms are determined with the aid of a procedure which was recently suggested by Davidson and Workman [8]. The advantage of this recipe over other schemes, is that the added contact terms do not contain any singularities. This is not the case for older procedures, such as those suggested by Ohta [9] or Haberzettl [10], which have been adopted in numerous theoretical works dealing with meson induced and meson production reactions.

Within the context of an effective-field theory, the degree of participation of the different intermediate resonances is determined by the magnitude of the corresponding electromagnetic and strong coupling constants. Those values are not predicted by the theory itself, but should be determined by comparing model calculations to an extensive data set. The most recently published $p(\gamma,K^+)\Sigma^0$ and $p(\gamma,K^0)\Sigma^+$ data are due to the SAPHIR Collaboration at the ELSA facility in Bonn [1,2]. This data set for Σ^0 (Σ^+) photoproduction contains 21 (5) total and 70 (18) differential cross section points, as well as 12 (4) recoil polarization asymmetries over an energy range from threshold up to 2.0 (1.55) GeV. On the basis of these data, we have determined the optimal coupling constants for several sets of intermediate resonances by minimizing χ^2, which is defined in the standard manner:

$$\chi^2=\frac{1}{N}\sum_{i=1}^{N}\frac{[X_i-Y_i(a_1,\ldots,a_n)]^2}{\sigma_{X_i}^2}. \tag{2}$$

Here, X_i are the measured observables, $\sigma_{X_i}^2$ their standard deviations, $Y_i(a_1,\ldots a_n)$ the theoretical predictions for the variables X_i and N the number of data points in the fit. The a_j's denote the free parameters (coupling constants and hadronic form-factor cutoffs) of the model.

The Σ^-, Σ^+, and Σ^0 baryons form an isospin triplet. As outlined in the Appendix, one can exploit isospin symmetry to establish relations between the hadronic and electromagnetic coupling constants for the different Σ photoproduction channels. The obvious advantage of such a procedure, is that the $p(\gamma,K^+)\Sigma^0$ and $p(\gamma,K^0)\Sigma^+$ data can be described with one common set of parameters. In principle, the $n(\gamma,K^0)\Sigma^0$ and $n(\gamma,K^+)\Sigma^-$ channels could also be implemented in this scheme [11]. Data for those reaction channels are sparse, though. Moreover, the procedure of extracting ''elementary'' neutron cross sections from measurements on nuclei, such as the deuteron, induces severe model dependences. To make matters even worse, connecting proton to neutron electromagnetic coupling constants demands the knowledge of the rather poorly known helicity amplitudes for the different nucleon resonances. For all of the above arguments, we have excluded from our global analyses the Σ photoproduction channels off the neutron.

Even at tree level, the description of $\gamma p\to KY$ processes involves a substantial number of Feynman diagrams. The diagrams can be divided into two broad classes, the background (or, nonresonant) and the resonant terms. The latter reflect themselves as s channel terms and are esteemed to contain the most relevant physical information. The extracted coupling constants for the corresponding resonant states constitute the bridge between the photoproduction measurements and quark-model predictions [12–14]. However, the implementation of the background contributions in the description of $\gamma p\to KY$ processes is far from being a trivial task. The background contains several classes of Feynman graphs. First the Born terms, involving an off-shell proton in the s channel, a K meson exchange in the t channel and hyperon exchange in the u channel. Second, there are terms involving the exchange of a K^* vector meson in the t channel and Y^* hyperon resonances in the u channel. Some models dealing with Λ and Σ photoproduction have neglected these resonant u channel terms [15,16]. The exchange of K^* and Y^* particles in the t and u channel are perceived as background and not as resonant diagrams, as they do not possess poles in the physical region of the reaction.

B. Born diagrams

It is a notable fact that the Born terms on their own exhibit rather intriguing characteristics when it comes to modeling the $\gamma p\to K^+\Lambda$ and $\gamma p\to K\Sigma$ reaction dynamics. The Born terms only depend on two parameters $g_{K^+\Lambda p}$ and $g_{K^+\Sigma^0 p}$, which are in principle strictly related to the well-determined $g_{\pi NN}$ coupling constant through SU(3) flavor symmetry. In practice, SU(3) is a broken symmetry and at best some ''realistic'' ranges for $g_{K^+\Lambda p}$ and $g_{K^+\Sigma^0 p}$ can be set. Reasonable ranges, corresponding with deviations of 20% from the SU(3) predictions, are

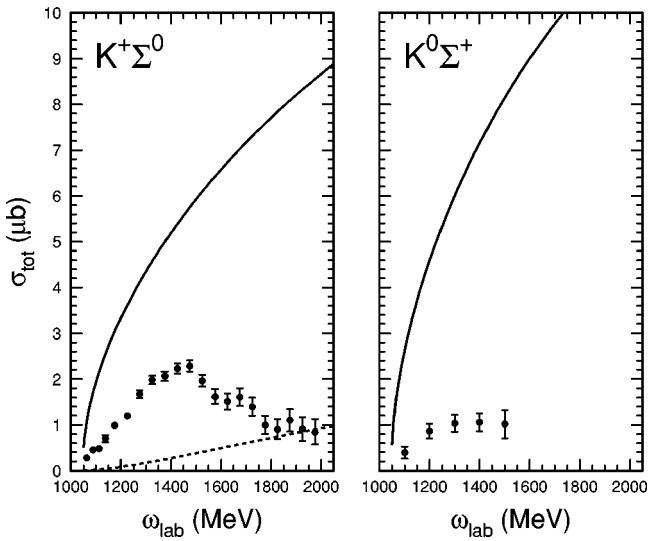

FIG. 1. The photon-energy dependence of the contribution from the Born diagrams to the total $p(\gamma,K^+)\Sigma^0$ and $p(\gamma,K^0)\Sigma^+$ cross sections. These results are obtained without introducing hadronic form factors and $g_{K^+\Lambda p}/\sqrt{4\pi}=-3.0$ and $g_{K^+\Sigma^0 p}/\sqrt{4\pi}=0.9$. The dashed curve in the $p(\gamma,K^+)\Sigma^0$ panel, is the result after excluding the ''extended'' Born term depicted in Fig. 2. The data are from Refs. [1,2].

$$-4.5 \leqslant \frac{g_{K^+\Lambda p}}{\sqrt{4\pi}} \leqslant -3.0, \tag{3a}$$

$$0.9 \leqslant \frac{g_{K^+\Sigma^0 p}}{\sqrt{4\pi}} \leqslant 1.3. \tag{3b}$$

Purely hadronic processes, such as KN scattering [17] or $pp \rightarrow pKY$ reactions [18,19], can be understood in terms of the SU(3)-based coupling constants. These observations may suggest that there is little room for SU(3) breaking beyond the aforementioned ranges. In the electromagnetic production of strangeness, though, a difficulty emerges [4,20–22]. Indeed, using coupling constants which vary within the aforementioned boundaries, the predicted strength from the ''bare'' Born terms overshoots the measured $p(\gamma,K^+)\Lambda$ cross section by a factor of 3 or 4. In the Σ photoproduction case, we observe similar qualitative features. The photon-energy dependence of the total $p(\gamma,K^+)\Sigma^0$ and $p(\gamma,K^0)\Sigma^+$ cross sections, calculated in a model that solely includes the Born terms, is displayed in Fig. 1. For both Σ production channels, the Born terms in themselves strongly overpredict the measurements. For the curves of Fig. 1 we adopt the values $g_{K^+\Lambda p}/\sqrt{4\pi}=-3.0$ and $g_{K^+\Sigma^0 p}/\sqrt{4\pi}=0.9$. They correspond with the smallest absolute couplings which are allowed according to Eq. (3). When adopting couplings based on exact SU(3) symmetry, the overprediction becomes even more severe.

An intriguing observation is that, under the constraints of Eq. (3), the major fraction of the Born strength in the $p(\gamma,K^+)\Sigma^0$ channel is stemming from the so-called ''extended'' Born diagram which is sketched in Fig. 2. In this diagram, a Λ is produced in the u channel and converted into a Σ^0 at the electromagnetic vertex. The dominance of this term can be attributed to the large value of $g_{K^+\Lambda p}$ compared to $g_{K^+\Sigma^0 p}$. As a matter of fact, this implies that the major part of the background cross section in Σ^0 production is dominated by Λ exchange in the u channel. Due to charge conservation, Λ exchange cannot contribute to the Born terms for Σ^+ photoproduction. In the $p(\gamma,K^0)\Sigma^+$ channel, the Born contributions consist only of proton exchange in the s channel and Σ^+ exchange in the u channel. Remark that also the t channel does not contribute since the photon does not couple to the neutral K^0 meson. Despite the restricted number of background diagrams, the two Born terms produce far more strength than in the Σ^0 photoproduction case. This can be partly attributed to the $g_{K^0\Sigma^+ p}$ coupling constant which is, according to the relation (A3), a factor of $\sqrt{2}$ larger than $g_{K^+\Sigma^0 p}$ and partly to the values of the corresponding anomalous magnetic moments ($\kappa_{\Sigma^+}=1.458$, $\kappa_{\Sigma^0}=0.79$) [23,24].

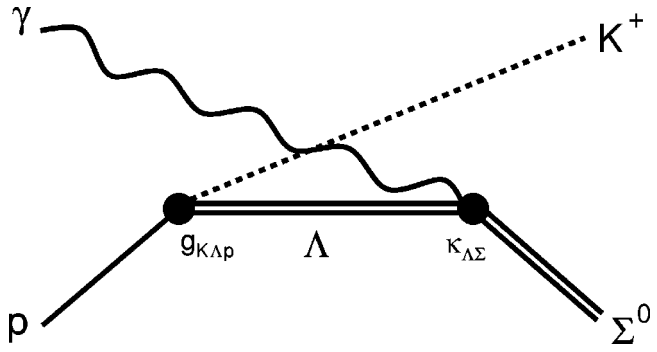

FIG. 2. The so-called ''extended'' Born term contributing to the $p(\gamma,K^+)\Sigma^0$ process. A Λ hyperon is exchanged in the u channel and converted into a Σ^0 at the electromagnetic vertex.

From the above discussion it may become clear that apart from introducing resonances, it is mandatory to add model ingredients that properly counterbalance the strength produced by the ''bare'' Born terms. In Λ photoproduction, where one comes across a similar difficulty, we discussed three schemes in which this goal could be accomplished [4]. First, it is well known that for sufficiently low values of the cutoff mass Λ in the hadronic form factors of Eq. (1), the strength stemming from the Born terms can be adequately suppressed without invoking other mechanisms. It turns out that in such a scheme an appropriate description of the Λ photoproduction data can solely be achieved with cutoff masses of the order of the kaon mass. This is a rather inconvenient situation for an effective-field theory. Second, in Ref. [25] we have shown that for the $p(\gamma,K^+)\Lambda$ process, the introduction of hyperon resonances (Λ* and Σ*) in the u channel permits one to naturally cut down the strength from the Born terms through destructive interferences. Such a scheme offers the obvious advantage of describing the photoproduction data with cutoff masses of a few times the kaon mass. As a third alternative, the constraints from (broken) SU(3)-flavor symmetry of Eq. (3) can be simply disregarded. It goes without saying that after sufficiently reducing the $g_{K^+\Lambda p}$ and $g_{K^+\Sigma^0 p}$ couplings, one can (artificially) force the strength from the Born diagrams to approach the magnitude

TABLE I. The table summarizes the reduced χ^2 values for the different sets of N^* and Δ^* resonances and a particular model to treat the background diagrams. The χ^2 values are from the best fits obtained from comparing the model calculations with the SAPHIR $p(\gamma,K)\Sigma$ data. With "N^* core set" we refer to the $S_{11}(1650)$, $P_{11}(1710)$, and $P_{13}(1720)$ nucleon resonances. NFP indicates the total number of free parameters in the corresponding fitting procedure.

Resonance contributions					Background	χ^2	NFP
N^*core set	$D_{13}(1895)$	$S_{31}(1620)$	$S_{31}(1900)$	$P_{31}(1910)$	Model		
◆					D	6.52	13
◆		◆	◆		D	4.16	15
◆		◆		◆	D	5.66	15
◆			◆	◆	D	3.20	15
◆		◆	◆	◆	D	3.19	16
◆	◆				D	5.29	18
◆	◆		◆	◆	D	2.88	20
◆			◆	◆	A	2.03	15
◆	◆		◆	◆	A	1.98	20
◆			◆	◆	B	1.95	17
◆	◆		◆	◆	B	1.81	22
◆			◆	◆	C	1.96	15
◆	◆		◆	◆	C	1.89	20

of the measured cross sections.

In this work, we extend our description of Λ photoproduction [4] to the Σ production channels. Building on the knowledge gained in Λ photoproduction, in Sec. III B we will present various schemes to implement the background diagrams in modeling $p(\gamma,K)\Sigma$ reactions. First, however, we will look for a proper set of resonances to describe the currently available $p(\gamma,K)\Sigma$ data in Sec. III A. Finally, in Sec. III C we consider the $p(K^-,\gamma)\Sigma^0$ reaction.

III. RESULTS

A. Resonance contributions

Recent isobar models [4,5,15,26] identified the three nucleon resonances $S_{11}(1650)$, $P_{11}(1710)$, and $P_{13}(1720)$ as leading N^* contributions to the $p(\gamma,K^+)\Lambda$ reaction. It thus appears natural to consider them as privileged candidates to participate in the Σ photoproduction channels [16]. On the other hand, we do not have similar guidelines concerning the leading Δ^* contributions. In our numerical investigations, we rely on a χ^2 procedure to judge whether a particular set of resonances is suited to describe the data. In the process of determining an optimum set of N^* and Δ^* particles, we have fixed a basic set consisting of the three aforementioned N^* resonances to which we have gradually added other combinations of N^* and Δ^* states. All results reported in this subsection are obtained with a particular model choice (in Sec. III B coined model D) for treating the background. A profound discussion of the implementation of the background diagrams is postponed to Sec. III B.

Starting with a "core set" consisting of the $S_{11}(1650)$, $P_{11}(1710)$ and $P_{13}(1720)$ resonances, we arrive at $\chi^2=6.52$ for an overall fit to the combined set of $p(\gamma,K^+)\Sigma^0$ and $p(\gamma,K^0)\Sigma^+$ cross section and polarization asymmetry data. This quality of agreement surely allows room for improvement and, consequently, for additional N^* and Δ^* resonances playing a non-negligible role in the reaction dynamics. Table I summarizes the attained χ^2 values for various combinations of resonances. In an attempt to minimize the number of free parameters, we started out with introducing only spin-1/2 Δ^* states. Note that in an effective Lagrangian approach, a spin-1/2 resonance adds only one free parameter while five extra parameters are introduced per spin-3/2 resonance (two coupling constants and three off-shell parameters). Candidates for spin-1/2 Δ^* resonances are the $S_{31}(1620)$, $S_{31}(1900)$, and $P_{31}(1910)$ states [23]. With those three Δ^* resonances and the aforementioned core of three N^* resonances consisting of the $S_{11}(1650)$, $P_{11}(1710)$, and $P_{13}(1720)$, we arrive at a global best fit with $\chi^2=3.19$. A similar quality of agreement ($\chi^2=3.20$), however, can already be achieved by the mere action of only two of these Δ^*'s, the $S_{31}(1900)$ and $P_{31}(1910)$. Other combinations selected out of the three aforementioned Δ^* states were also able to improve the description of the data (see Table I) although the combination of the $S_{31}(1900)$ and $P_{31}(1910)$ clearly produced the best χ^2. Note that these two Δ^* resonances were also recognized as most likely $I=\frac{3}{2}$ resonance candidates by Mart in his analysis of the Σ photoproduction data [16].

The recent $p(\gamma,K^+)\Lambda$ data from the SAPHIR Collaboration [1] exhibit a structure in the energy dependence about $\omega_{\rm lab}\approx 1.5$ GeV. In the analysis of Ref. [15], this structure was put forward as possible evidence for the existence of a "missing" $D_{13}(1895)$ resonance. An alternative interpretation in terms of the exchange of a spin-3/2 Λ^* resonance in the u channel was put forward by Saghai in Ref. [26]. In Ref. [4], we stressed that N^* resonances with other quantum numbers can also account for the observed structure. From this discussion it may already become obvious that the identification of "missing resonances" and their properties from

strangeness photoproduction data, is a heavily debated topic. We have investigated in how far the inclusion of a ''missing'' $D_{13}(1895)$ resonance improves the fits of the Σ photoproduction data. Including the core set of three N^*'s and the $D_{13}(1895)$ in the *s* channel, we arrive at a best fit with $\chi^2 = 5.29$. Despite the fact that the D_{13} and Δ^* resonances have their poles in the same energy region, inspection of Table I learns that this quality of agreement is inferior to what was obtained in the calculation with two Δ^* resonances. A resonance set consisting of the core of three N^* resonances, the D_{13} and the two Δ^*'s leads to a fit with $\chi^2 = 2.88$. Compared to the χ^2 of 3.20, achieved without introducing the D_{13}, this represents only a minor improvement, in view of the fact that the introduction of a spin-3/2 resonance comes at the expense of throwing in five additional free parameters in the fitting procedure.

Summarizing the findings of Table I, we are tempted to conclude that Δ^* resonances seem to constitute an essential part of the dynamics of Σ photoproduction. No convincing evidence for a salient role for the $D_{13}(1895)$ resonance in Σ photoproduction is found. In this subsection, we have drawn our conclusions on the basis of numerical calculations within one particular model (''model D'') for treating the background diagrams. Alternative models for implementing the background diagrams will be introduced in the forthcoming section. Anticipating these investigations, the relative role of the different N^* and Δ^* particles turns out to be rather independent of the choices made with respect to the treatment of the nonresonant diagrams. As it happens, this will turn out not always to be the case for the extracted quantitative resonance information.

B. Background contributions

As alluded to in Sec. II B, one of the long-standing issues in modeling strangeness photoproduction is the unrealistically large amounts of strength produced by the ''bare'' Born terms. In the process of trying to counterbalance the strength from these amplitudes by adding extra ingredients to the theory, it appears that some model dependence in the treatment of the background terms cannot be avoided. We now discuss four models which all succeed in cutting down the background strength in Σ photoproduction. In all schemes, the background contains at least the usual Born terms [including the ''extended'' diagram in the $p(\gamma,K^+)\Sigma^0$ case] and the $K^*(892)$ vector-meson exchange in the *t* channel. For the investigations presented in this subsection, the resonant part includes the N^* resonances $S_{11}(1650)$, $P_{11}(1710)$, and $P_{13}(1720)$ and the Δ^* states $S_{31}(1900)$ and $P_{31}(1910)$. Those five resonances were identified in Sec. III A as an appropriate set for describing Σ photoproduction with a minimal number of free parameters.

Model A. The hadronic form factors $F_x(\Lambda)$, described in Eq. (1), cut the high-momentum dependence of the different amplitudes and emerge as a mechanism to reduce the strength stemming from the Born diagrams to magnitudes of the order of the measured cross sections. To fully exploit the power of this reduction mechanism, we imposed an under limit of 0.4 GeV for the cutoff mass Λ during the fit. Thereby, no Y^* contributions in the *u* channel are considered. Despite our reservations regarding the use of ''soft'' cutoff masses, eventually we arrive in this scheme at a very satisfactory $\chi^2 = 2.03$ with a cutoff mass Λ close to the under limit of 0.4 GeV. It should be stressed that with cutoff masses as small as the kaon mass, the hadronic form factor starts playing a predominant role in the description of the reaction dynamics and heavily affects the predicted values of the observables, not only in the high-energy regime but even at threshold.

Model B. In Ref. [25], we pointed out that for the description of $p(\gamma,K^+)\Lambda$ processes, the introduction of hyperon resonances in the *u* channel can be an efficient and physically relevant way of counterbalancing the strength produced by the Born terms. More specifically, the destructive interference between the *u* channel amplitudes of the $\Lambda^*(1800)$ and $\Lambda^*(1810)$ hyperon resonances and the Born terms resulted in a very satisfactory description of the $p(\gamma,K^+)\Lambda$ data. We have made an attempt to identify an equivalent procedure for $K\Sigma$ photoproduction. Unfortunately, there is relatively little theoretical guidance on how to select the proper intermediate hyperon resonances and how to determine realistic values for their coupling constants. Nevertheless, after including the $\Lambda^*(1810)$ and $\Sigma^*(1880)$ in the *u* channel, we arrive at a fair description of the $p(\gamma,K^+)\Sigma^0$ and $p(\gamma,K^0)\Sigma^+$ data with a χ^2 of 1.95.

Note that the Λ^* resonance does not feed the $\gamma p \rightarrow K^0\Sigma^+$ channel. Consequently, the procedure of introducing hyperon resonances in the *u* channel, as a natural physical mechanism to counteract the background amplitudes, is expected to be less effective in the $p(\gamma,K^0)\Sigma^+$ channel. However, as can be seen in Fig. 3, a stronger destructive interference between the K^* vector-meson contribution in the *t* channel and the background diagrams is noted for the $p(\gamma,K^0)\Sigma^+$ process. One may wonder why this mechanism does not seem to prevail so strongly in the Σ^0 photoproduction case. This can be naturally explained by looking at the respective electromagnetic coupling constants of the K^* vector mesons. On the basis of Eq. (A10), one finds that the loss of destructive interference with the Λ^* resonance in the $p(\gamma,K^0)\Sigma^+$ process is likely to be counterbalanced by an enhanced destructive interference with the *t* channel vector-meson exchanges.

One of the obvious advantages of the ''model B'' described here, is that the role of the hadronic form factors can be diminished to levels that appear physically acceptable. Indeed, good fits ($\chi^2 = 1.95$) of the Σ photoproduction data can be obtained with a ''hard'' cutoff mass of the order $\Lambda = 1.6$ GeV. One argument that may speak against model B is that the extracted values of the Y^* coupling constants turn out to be large in comparison with the N^* and Δ^* coupling strengths. However, the two *u* channel particles, introduced in the computations, could be interpreted as representing effective particles which account for a larger set of *u* channel processes [4].

Model C. A third option is to simply disregard the constraints of Eq. (3) imposed by (broken) SU(3)-flavor symmetry. Then, the $g_{K^+\Lambda p}$ and $g_{K^+\Sigma^0 p}$ coupling constants can be

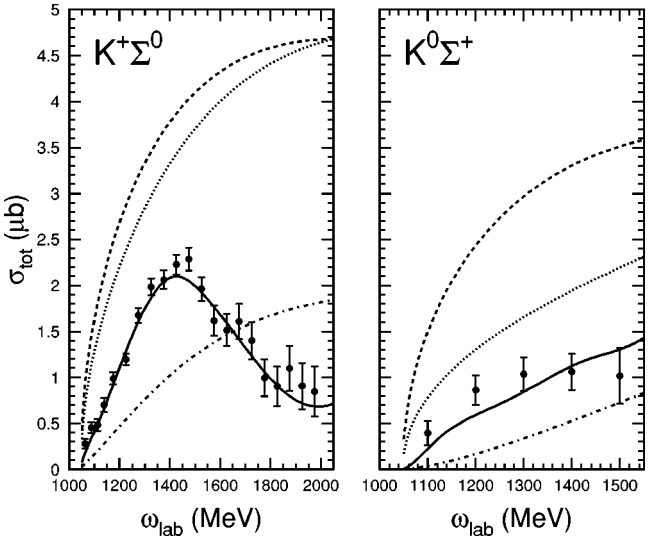

FIG. 3. Total cross sections for the $p(\gamma,K^+)\Sigma^0$ and $p(\gamma,K^0)\Sigma^+$ processes. The dashed curve denotes the computed strength from the Born terms (with ''strong'' hadronic form factors $\Lambda=1.6$ GeV). For the dotted line, the K^* t channel contribution is added. The dot-dashed curve includes the Y^* hyperon resonances and consequently is the result of the full background contribution as computed within model B. The solid line embodies, in addition to the background, the s channel N^* and Δ^* resonances. The data are from Refs. [1,2].

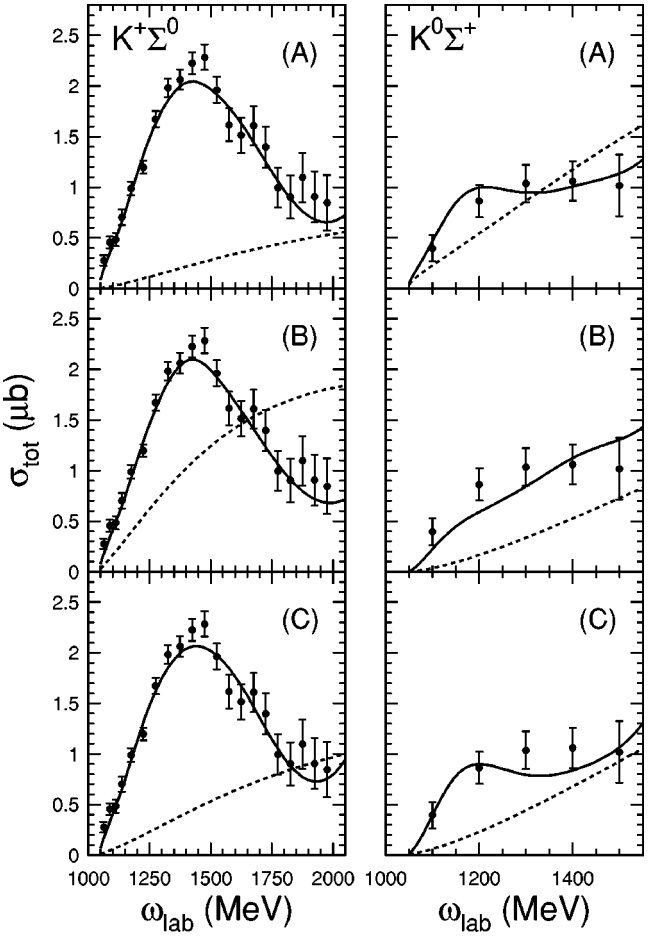

FIG. 4. Energy dependence of the total $p(\gamma,K^+)\Sigma^0$ and $p(\gamma,K^0)\Sigma^+$ cross sections. The dashed curves denote the computed strength from the ''background'' diagrams. The solid curves include both the background and the resonant amplitudes. The panels (A), (B), (C) refer to the optimum fits obtained with the three background models A, B, and C, respectively. The data are from Refs. [1,2].

treated as free parameters in the minimization procedure. In calculations with model C we are solely constraining the relative sign between the two coupling constants. Ignoring Y^* exchange in the u channel, we arrive at an overall agreement with the data of $\chi^2=1.96$ with $g_{K^+\Lambda p}/\sqrt{4\pi}=-0.23$ and $g_{K^+\Sigma^0 p}/\sqrt{4\pi}=0.28$. These numbers are dramatically smaller than what is predicted on the basis of SU(3)-flavor symmetry (-3.75 and 1.09, respectively). In this fit, the cutoff mass was allowed to vary freely and adopts a value of 2.5 GeV. This value of Λ alludes to a rather modest role for the hadronic form factors in the description of the reaction dynamics.

Model D. This scheme is an attempt to unite some of the virtues of the three models presented above, at the same time minimizing the number of free parameters that are introduced to compute the background diagrams. In this model, the constraints of Eq. (3) are respected during the fitting procedure. In an attempt to keep the model as simple as possible, no Y^* particles in the u channel are introduced. The hadronic cutoff mass Λ is treated as a parameter and allowed to vary freely in a range defined by the under limit 1.1 GeV. In the optimum fit, the value of Λ always approaches this under limit, stressing the essential role of the hadronic form factors for keeping the strength from the Born diagrams at realistic levels. In Sec. III A this scheme for treating the background diagrams was adopted when investigating the dominant resonance contributions. This choice was made on the basis of a minimized number of free parameters related to the background diagrams. Inspecting Table I, it becomes obvious, though, that for a fixed set of resonances model D systematically leads to χ^2 values which are inferior to those obtained in models A, B, and C.

With all suggested models for implementing the background diagrams, we arrive at a satisfactory description of the available data. This feature becomes apparent from the χ^2 values contained in Table I and can also be illustrated by directly comparing model predictions with the data points. Figure 4 shows the energy dependence of the total cross section for the background models A, B, and C. In these plots, the strength from the background diagrams is also shown. It is clear from this figure that the predictions for the background and resonant strength are qualitatively similar for models A and C. Nevertheless, there are major differences between the assumptions underlying the two models. Most importantly, whereas model A is based on g_{KYp} coupling constants respecting (broken) SU(3) flavor symmetry, model C does not impose any constraints of that type. However, it appears that respecting SU(3) flavor symmetry comes at a certain price. Indeed, when adopting SU(3) constraints on the g_{KYp} values, one appears to be forced to either introduce (unrealistically) soft hadronic form factors (model A),

TABLE II. Numerical values of the coupling constants and hadronic cutoff masses (in MeV) in the isobar model calculations for the $p(\gamma,K^+)\Sigma^0$ process. The conventions for the coupling constants are as in Ref. [4].

		model A	model B	model C
Born terms	$g_{K^+\Sigma^0 p}/\sqrt{4\pi}$	9.949×10^{-1}	9.215×10^{-1}	2.811×10^{-1}
	$g_{K^+\Lambda p}/\sqrt{4\pi}$	-4.487	-3.017	-2.261×10^{-1}
K^*	$G^v_{K^*}$	6.926×10^{-2}	7.598×10^{-2}	6.828×10^{-2}
	$G^t_{K^*}$	8.047×10^{-2}	4.087×10^{-2}	1.411×10^{-1}
$P_{01}(1810)$	$G_{P_{01}}$		21.838	
$P_{11}(1880)$	$G_{P_{11}}$		-9.451	
$S_{11}(1650)$	$G_{S_{11}}$	-4.568×10^{-2}	-4.516×10^{-3}	-2.511×10^{-2}
$P_{11}(1710)$	$G_{P_{11}}$	-1.213×10^{-1}	-1.583×10^{-1}	-1.879×10^{-1}
$P_{13}(1720)$	$G^{(1)}_{P_{13}}$	2.367×10^{-2}	1.706×10^{-2}	2.699×10^{-2}
	$G^{(2)}_{P_{13}}$	5.238×10^{-2}	8.343×10^{-2}	5.213×10^{-2}
	$X_{P_{13}}$	12.351	6.943	14.863
	$Y_{P_{13}}$	3.781	4.765	3.861
	$Z_{P_{13}}$	-1.122	-1.129	-1.089
$S_{31}(1900)$	$G_{S_{31}}$	5.131×10^{-2}	4.279×10^{-2}	4.351×10^{-2}
$P_{31}(1910)$	$G_{P_{31}}$	3.726×10^{-1}	3.599×10^{-1}	3.920×10^{-1}
cutoff mass	Λ_{born}	439.68	1605.04	2509.22
	Λ_{res}	1616.20	1602.43	1601.54
χ^2		2.03	1.95	1.96

or implement additional u channel diagrams (model B) to destructively interfere with the Born terms. In the literature on $p(\gamma,K)Y$, there is no agreement on whether or not to respect SU(3) symmetry. The analysis of Lee *et al.* in Ref. [27] is based on moderately broken SU(3) symmetry ($g^+_{K\Lambda p}/\sqrt{4\pi}=-3.80$ and $g^+_{K\Sigma p}/\sqrt{4\pi}=1.20$). This for example also holds for the work of David *et al.* [28] ($g^+_{K\Lambda p}/\sqrt{4\pi}=-3.23$ and $g_{K\Sigma p}/\sqrt{4\pi}=0.80$). Other analyses yielded g_{KYp} coupling constants which do not respect SU(3) symmetry. Williams *et al.* [20] were one of the first to document that by not imposing flavor symmetry a fair description is obtained with much smaller couplings $-2.38 \leqslant g^+_{K\Lambda p}/\sqrt{4\pi} \leqslant -1.16$ and $0.0928 \leqslant g^+_{K\Sigma^0 p}/\sqrt{4\pi} \leqslant 0.273$. Similarly and more recently, Mart *et al.* [11] use $g^+_{K\Lambda p}/\sqrt{4\pi}=0.51$ and $g^+_{K\Sigma^0 p}/\sqrt{4\pi}=0.13$, Feuster and Mosel [5] extract $g^+_{K\Lambda p}/\sqrt{4\pi}=-1.72$ and Hsiao *et al.* [22] arrives at values ranging between $-2.41 \leqslant g^+_{K\Lambda p}/\sqrt{4\pi} \leqslant -1.24$ and $-0.50 \leqslant g^+_{K\Sigma^0 p}/\sqrt{4\pi} \leqslant 1.04$. All these absolute g_{KYp}'s are substantially smaller than what could be expected on the basis of moderately broken SU(3) flavor symmetry. The numerical values obtained in this work are summarized in Table II. As pointed out in Ref. [5], it probably makes more sense to compare the product $g_{KYp}\cdot\hat{F}$ than the bare coupling constants g_{KYp}. In this respect, our model A, based on SU(3) flavor symmetry for g_{KYp}, requires form factors $\hat{F}$ of the order 0.1. Model C, on the other hand, use values of $\hat{F}$ of the order 1, but the g_{KYp} are close to one-tenth of the SU(3) predictions. This results in comparable values for $g_{KYp}\cdot\hat{F}$ in both models. In model B, SU(3) flavor symmetry is only mildly violated and due to the larger cutoff mass, the product $g_{KYp}\cdot\hat{F}$ is considerably larger than in the models A and C.

In Fig. 5, model calculations for the angular distribution of the $p(\gamma,K^+)\vec{\Sigma}^0$ and $p(\gamma,K^0)\vec{\Sigma}^+$ recoil-polarization asymmetry are given. This asymmetry is defined as

$$P=\frac{d\sigma/d\Omega^{(+)}-d\sigma/d\Omega^{(-)}}{d\sigma/d\Omega^{(+)}+d\sigma/d\Omega^{(-)}}, \tag{4}$$

where $+(-)$ refers to a hyperon polarization parallel (anti parallel) to the $(\vec{p}_\gamma\times\vec{p}_K)$ axis. Note, however, that the data points for the asymmetry of the $K^0\Sigma^+$ process, are binned over the whole energy range. Consequently, they hardly affect the χ^2 of the global fit.

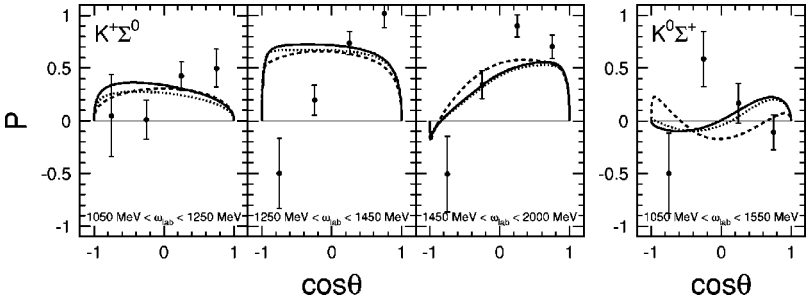

FIG. 5. Angular dependence of the $p(\gamma,K^+)\vec{\Sigma}^0$ and $p(\gamma,K^0)\vec{\Sigma}^+$ recoil-polarization asymmetry (P). The solid, dashed, and dotted lines are obtained with background model A, B, and C, respectively. Our results are averaged over the experimental energy bins. The data are from Refs. [1,2].

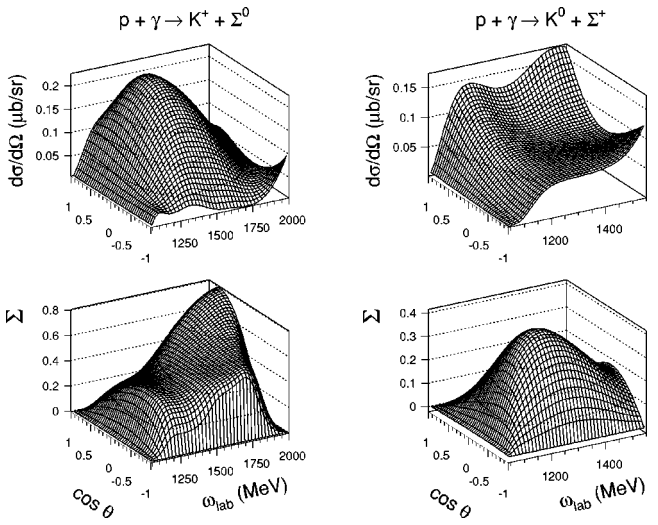

FIG. 6. The differential cross section and photon-beam asymmetry (Σ) for the $p(\gamma,K^+)\Sigma^0$ and $p(\gamma,K^0)\Sigma^+$ processes as a function of the photon lab energy $\omega_{\rm lab}$ and cos θ. The calculations account for the $S_{11}(1650)$, $P_{11}(1710)$, $P_{13}(1720)$, $S_{31}(1900)$, and $P_{31}(1910)$ s channel resonances. The background terms are treated according to the prescriptions of model A.

Predictions for the energy and angular dependence of the differential cross section and the photon-beam asymmetry (Σ) are displayed in Figs. 6, 7, and 8 for the models A, B, and C described above. The photon-beam asymmetry is defined in the standard manner:

$$\Sigma = \frac{d\sigma/d\Omega^{(\perp)} - d\sigma/d\Omega^{(\parallel)}}{d\sigma/d\Omega^{(\perp)} + d\sigma/d\Omega^{(\parallel)}}. \tag{5}$$

Here, $\perp(\parallel)$ refers to linearly polarized photons perpendicular (parallel) to the reaction plane. From visual inspection of the Figs. 6–8, it indeed becomes apparent that the energy and angular dependence of the differential cross sections is rather similar for the three models. The sudden rise in the predicted Σ^0 cross sections at very backward angles and the highest photon energies should not be considered as physical. It illustrates the limits of the hadronic models for predicting observables in ''unmeasured'' regions of the phase space. Note that the data used in the fitting procedure do not extend beyond 2.0 GeV (Σ^0 production) and 1.55 GeV (Σ^+ production). For the angular and energy dependence of the $p(\vec{\gamma},K^+)\Sigma^0$ photon-beam asymmetry, models A, B, and C produce comparable results. Although no published data exist for this observable to date, the model dependences in the predictions for this observable seem to be modest. On the other hand, large variations between the different predictions for the $p(\gamma,K^0)\Sigma^+$ photon-beam asymmetry are observed. To fully appreciate this, we have gathered the calculations for the photon-beam asymmetries at some fixed photon lab energies in Fig. 9. With no doubt, more precise data for the various polarization observables would help in further constraining the model dependences in the treatment of the background diagrams.

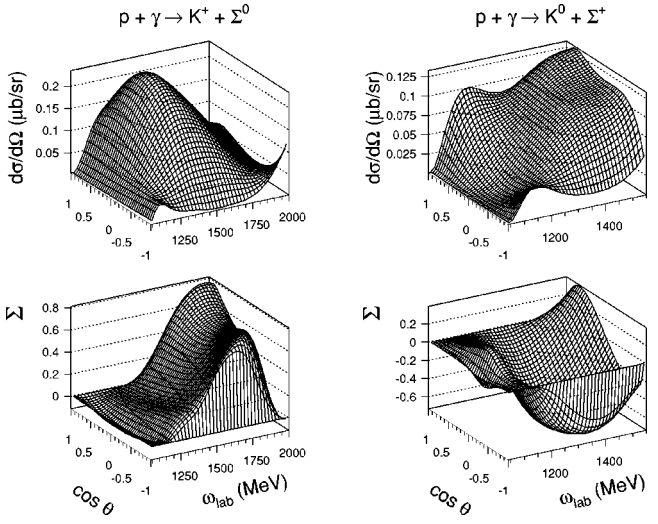

FIG. 7. As in Fig. 6 but now for background model B.

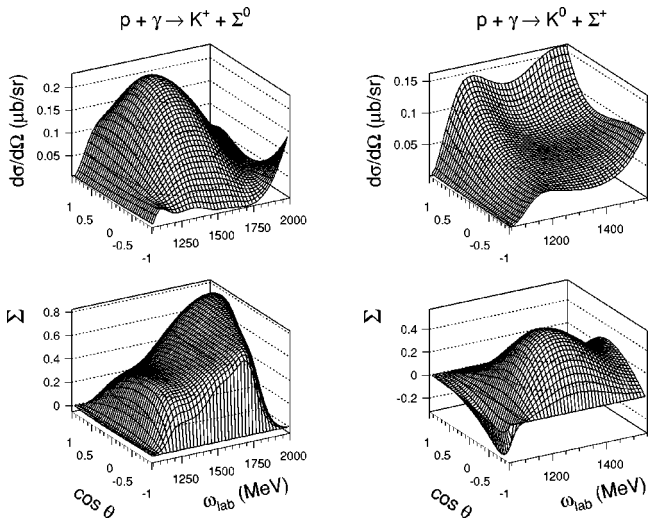

FIG. 8. As in Fig. 6 but now for background model C.

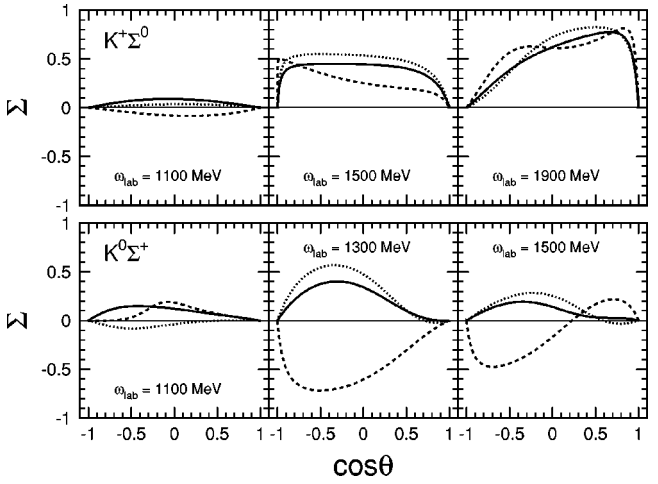

FIG. 9. The angular dependence of the photon-beam asymmetry (Σ) for three photon lab energies. The solid, dashed, and dotted curves are the predictions as obtained with the background models A, B, and C, respectively. The upper panels are for the $p(\vec{\gamma},K^+)\Sigma^0$ process, the lower for the $p(\vec{\gamma},K^0)\Sigma^+$ reaction.

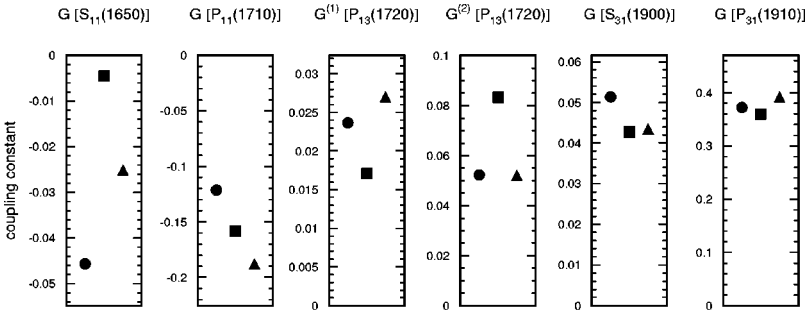

FIG. 10. The extracted coupling constants for the N^* and Δ^* resonances. The circles are extracted within model A, the squares within model B, and the triangles within model C. The conventions adopted for the coupling constants are summarized in Ref. [4].

Not only the predictions for some of the asymmetries, but also the extraction of resonance parameters, turns out to be reasonably sensitive to the adopted procedure to treat the background. This feature is illustrated in Fig. 10, where the extracted resonance coupling constants are plotted for the background models A, B, and C. For the $I=\frac{3}{2}$ Δ^* resonances, the extracted coupling constants are rather insensitive to the choices for the background. Larger variations, exceeding the 20% level are observed for the extracted N^* parameters. Table II lists the numerical values of all parameters corresponding with the optimum fits. The discerned model variation in the resonance parameters show that a model-independent extraction of this information from the strangeness-photoproduction data is not yet at hand. This is rather unfortunate, given that these variables play a crucial role in linking the predictions of (constituent) quark models and the photoproduction data.

To conclude this section, we come back to the aforementioned issue of the missing D_{13} nucleon resonance. Adopting background model D, the inclusion of this N^* particle improved the quality of the global fit from $\chi^2=3.20$ to $\chi^2=2.88$. We stress again that this comes at the expense of adding five extra parameters. We have investigated whether a similar qualitative feature emerged with background models A, B, and C. In all cases, a global fit with the core of the three N^* and the two Δ^* resonances with and without the $D_{13}(1895)$ was performed. The results are contained in Table I. The improvement in the quality of the fit varied from 3% (model A) to 8% (model B). We appreciate this improvement as rather modest in view of the five extra parameters. For the sake of reference, we mention that in a comparable tree-level analysis of the $p(\gamma,K^+)\Lambda$ data, the inclusion of an extra $D_{13}(1895)$ resonance improved the fits from 22 up to 40%, depending on the choices made for computing the background contributions [25].

C. Radiative kaon capture

Through the rules of crossing symmetry [29], the process of radiative kaon capture,

$$K^-+p\rightarrow\gamma+\Sigma^0, \tag{6}$$

is related to the kaon photoproduction $p(\gamma,K^+)\Sigma^0$ process. Indeed, one has

$$\mathcal{M}^{K^-p\rightarrow\gamma\Sigma^0}(p,k,p_K,p_\Sigma)=\mathcal{M}^{\gamma p\rightarrow K^+\Sigma^0}(p,-k,-p_K,p_\Sigma), \tag{7}$$

where p, k, p_K, and p_Σ are the four momenta of the proton, photon, kaon, and Σ, respectively. Unfortunately, to our knowledge the sole reliable data point for the radiative kaon capture process is for the branching ratio of *stopped* kaons

$$\mathcal{R}=\frac{\Gamma(K^-p\rightarrow\gamma\Sigma^0)}{\Gamma(K^-p\rightarrow\text{all})}$$
$$=\frac{\pi}{2W_{K^-p}}\frac{\omega}{M_pM_K(M_p+M_K)}\frac{1}{(4\pi)^2}$$
$$\times\frac{1}{2}|\mathcal{M}^{\gamma p\rightarrow K^+\Sigma^0}(p,-k,-p_K,p_Y)|^2, \tag{8}$$

where ω is the c.m. photon energy and $W_{K^-p}=560\pm135$ MeV fm^3 is the K^-p pseudopotential determined by Burkhardt *et al.* [30].

Our model predictions for $\mathcal{R}$ are summarized in Table III. It becomes clear that the three proposed background models produce values which differ by two orders of magnitude and considerably underestimate the measured value. However, it has been stressed by various authors [28,30,32] that the $\Lambda^*(1405)$ resonance, which is an s channel resonance just below the decay threshold, is of crucial importance for reproducing $\mathcal{R}$. In the Σ photoproduction process, the $\Lambda^*(1405)$ is a candidate for a resonant u channel contribution. However, in our analysis of $\gamma p\rightarrow K\Sigma$, no direct need for introducing the $\Lambda^*(1405)$ emerged (model B is the sole model that implements u channel Λ^* and Σ^* resonances). Therefore, we investigated whether a consistent description of the branching ratio $\mathcal{R}$ and the $p(\gamma,K)\Sigma$ SAPHIR data is feasible. To this end, we started out from background model B to which we added the $\Lambda^*(1405)$ hyperon resonance. In the fitting procedure against the SAPHIR data and the value of $\mathcal{R}$, we arrive at a χ^2 value of 1.92. The result for $\mathcal{R}=1.56\times10^{-3}$ is in agreement with the experimental value within the error bars.

TABLE III. Model predictions with the background models A, B, and C for the branching ratio $\mathcal{R}=\Gamma(K^-p\rightarrow\gamma\Sigma^0)/\Gamma(K^-p\rightarrow\text{all})$. The experimental value is from Ref. [31].

	A	B	C	B + $\Lambda^*(1405)$	experiment Ref. [31]
$\mathcal{R}\times10^3$	0.016	0.259	0.002	1.556	$1.44\pm0.20\pm0.11$

To conclude this subsection, we wish to stress that the branching ratio $\mathcal{R}$ in radiative kaon capture has only a limited potential to constrain the $p(\gamma,K)\Sigma$ reaction dynamics. Indeed, there are strong indications that the value of $\mathcal{R}$ is mainly determined by the strength of the $\Lambda^*(1405)$ while this resonance plays only a secondary role in $\gamma p \to K\Sigma$ reactions.

IV. CONCLUSION

In this work, we have presented results for neutral and charged Σ photoproduction off the proton in a hadronic model at tree level. By comparing model calculations to the SAPHIR data, we were able to identify a set of five N^* and Δ^* resonances [$S_{11}(1650)$, $P_{11}(1710)$, $P_{13}(1720)$, $S_{31}(1900)$, and $P_{31}(1910)$] with which a satisfactory description of the data can be obtained. Our calculations do not provide evidence for a salient role for the $D_{13}(1895)$ resonance in Σ photoproduction. The $D_{13}(1895)$ has never been observed in πN scattering. Recently, it was claimed that signals for the existence of such a resonance emerge from the Λ photoproduction data.

We have shown that the ''bare'' Born amplitudes produce $p(\gamma,K)\Sigma$ cross sections which dramatically overshoot the measured ones. Therefore, additional ingredients in the model calculations beyond resonance contributions appear essential. We have presented total and differential cross sections as well as recoil and photon asymmetry results for four schemes which accomplish to cut down satisfactorily the magnitude of the Born amplitudes. Through the background diagrams some model dependence in the extracted resonance parameters gets introduced. This dependence turns out to be small for the Δ^* particles. For some of the N^* resonances, though, the obtained coupling constants may vary substantially, depending on which model is used to implement the background. Predictions for the $p(\gamma,K^+)\Sigma^0$ photon-beam asymmetry are only moderately sensitive to the implementation of the background terms. This is not the case for the photon-beam asymmetries in the $p(\gamma,K^0)\Sigma^+$ channel. It should be stressed that for the Σ^0 case far more data are presently available. In the foreseeable future, the available amount of Σ photoproduction data in the resonance region will dramatically increase. Research efforts at Jefferson Lab [33], at GRAAL (Grenoble) [34], and SPring-8 [35] and continuing analysis work from the SAPHIR Collaboration [36] will extend the Σ and Λ photo production and electroproduction data beyond 2.0 GeV and will shed light on the (in)capability of hadronic approaches to model the physics at higher photon energies. They will also provide large and accurate sets of polarization data. With such an extended data base, one can be hopeful to better constrain the theoretical models and reveal the full dynamics of strangeness photoproduction reactions.

ACKNOWLEDGMENTS

This work was supported by the Fund for Scientific Research–Flanders under Contract No. 4.0061.99 and the Research Council of Ghent University.

APPENDIX: ISOSPIN SYMMETRY AND COUPLING CONSTANTS

Isospin symmetry considerations are extremely useful tools to establish ranges and relative signs between series of coupling constants. In this appendix we sketch how isospin arguments can be used to establish relations between the different hadronic and electromagnetic coupling constants which are required in global fits to photoinduced open strangeness production on the proton. In this appendix, we assume the isospin symmetry of the various meson and baryon multiplets to be exact. In what follows we will briefly address both hadronic and electromagnetic coupling constants.

1. Hadronic decays of N^* and Δ^* resonances

The calculation of hadronic transitions of baryon resonances poses a challenging task to constituent quark models (CQM). The major difficulty of such models is to determine the structure of the operators which govern the decay mechanism. This reflects the insufficient basic insight into the quark dynamics in low-energy hadron phenomenology. Most CQM's studying hadronic decays of baryon resonances (for a recent example, see Ref. [37]), start from a transition operator at quark level which does not contain isospin-dependent terms. In such a model, the amplitude for a pseudo-scalar hadronic decay of the type

$$B(I_1,M_1) \to K(I_2,M_2) + Y(I_3,M_3), \tag{A1}$$

is proportional to the isospin part

$$\frac{(-1)^{I_2-I_1}}{\sqrt{2I_1+1}} \langle I_2 M_2 I_3 M_3 | I_1 M_1 \rangle \langle I_2 \| \hat{T}^{(I_3)} \| I_1 \rangle, \tag{A2}$$

where I_i and M_i are the isospin and isospin projection of the respective particles and $\hat{T}^{(I)}$ denotes a spherical tensor operator of rank I. From the expression (A2), one easily obtains the following relations between the different isospin channels in $N \to K\Sigma$:

$$g_{K^+\Sigma^0 p} = \frac{g_{K^0\Sigma^+ p}}{\sqrt{2}} = -g_{K^0\Sigma^0 n} = \frac{g_{K^+\Sigma^- n}}{\sqrt{2}}. \tag{A3}$$

In determining these relations we adopted the following conventions for the isospin states of the *physical* Σ particles:

$$\begin{aligned} \Sigma^+ &: -|I=1,M=+1\rangle, \\ \Sigma^0 &: +|I=1,M=0\rangle, \\ \Sigma^- &: +|I=1,M=-1\rangle. \end{aligned} \tag{A4}$$

For the hadronic decays of the type $N \to K\Lambda$, starting from Eq. (A2), even simpler relations can be written down:

$$g_{K^+\Lambda p} = g_{K^0\Lambda n}. \tag{A5}$$

We now consider hadronic decays of the type $\Delta \to K\Sigma$. Defining the corresponding isospin states for the $\Delta^{+,0}$ particles as $|I=\frac{3}{2}, I_3=\pm\frac{1}{2}\rangle$, one obtains the following relations from Eq. (A2):

$$g_{K^+\Sigma^0\Delta^+} = -\sqrt{2}\, g_{K^0\Sigma^+\Delta^+}$$
$$= g_{K^0\Sigma^0\Delta^0} = \sqrt{2} g_{K^+\Sigma^-\Delta^0}. \quad \text{(A6)}$$

The relations contained in Eqs. (A3), (A5), and (A6), also hold when a N^*, K^*, Σ^*, or Λ^* resonance is involved at the vertex.

2. Electromagnetic vertices

Most of the information with respect to electromagnetic couplings rely on experimental quantities. The measured decay widths for the $K^{*+}(892)$ and $K^{*0}(892)$ vector mesons are [23]

$$\Gamma_{K^{*+}\to K^+\gamma} = 50 \pm 5 \ \text{keV}, \quad \text{(A7)}$$

$$\Gamma_{K^{*0}\to K^0\gamma} = 116 \pm 10 \ \text{keV}. \quad \text{(A8)}$$

In principle, one can determine the value of the magnetic transition moment on the basis of the proportionality $\kappa^2_{K^*K} \sim \Gamma_{K^*\to K\gamma}$. Within the context of isobar models, however, the coupling constants are frequently considered as ''effective couplings'' wherein, for example, part of final-state interaction effects are absorbed. It is a common procedure to use only the ratios of the measured decay widths to connect isospin related coupling constants. This leads to the following expression:

$$\frac{\kappa^2_{K^{*0}K^0}}{\kappa^2_{K^{*+}K^+}} = \frac{\Gamma_{K^{*0}\to K^0\gamma}}{\Gamma_{K^{*+}\to K^+\gamma}} \quad \text{(A9)}$$

or

$$\kappa_{K^{*0}K^0} = -1.52\kappa_{K^{*+}K^+}. \quad \text{(A10)}$$

The relative sign in the last expression was allocated on the basis of a CQM prediction [38].

The nucleon magnetic transition moments are related to the photohelicity amplitudes through the interaction Lagrangians. From the isospin structure of the N^* helicity amplitudes, it is easily proven that they are sensitive to the isospin of the final state. To determine the electromagnetic vertex coupling at a neutron target from the knowledge of the electromagnetic coupling at a proton target, those differences have to be taken into account. We adopt the same procedure as for the vector-meson transition moments and use the experimental amplitudes as a conversion coefficient. The expressions, which directly follow from the interaction Lagrangians, read

$$\text{spin}-\frac{1}{2}: \frac{\kappa_{N^*n}}{\kappa_{N^*p}} = \frac{A^n_{1/2}}{A^p_{1/2}}, \quad \text{(A11)}$$

$$\text{spin}-\frac{3}{2}: \frac{\kappa^{(1)}_{N^*n}}{\kappa^{(1)}_{N^*p}} = \frac{\sqrt{3}A^n_{1/2} \pm A^n_{3/2}}{\sqrt{3}A^p_{1/2} \pm A^p_{3/2}}, \quad \text{(A12)}$$

$$\frac{\kappa^{(2)}_{N^*n}}{\kappa^{(2)}_{N^*p}} = \frac{\sqrt{3}A^n_{1/2} - \dfrac{M_p}{M_{N^*}} A^n_{3/2}}{\sqrt{3}A^p_{1/2} - \dfrac{M_p}{M_{N^*}} A^p_{3/2}}, \quad \text{(A13)}$$

where $\pm$ refers to even/odd parity. Note that some of these helicity amplitudes are rather poorly known, especially those of the neutron. For the electromagnetic decay of the Δ^* resonances the following simple relation holds:

$$\kappa_{\Delta^*p} = \kappa_{\Delta^*n}, \quad \text{(A14)}$$

regardless of the spin state of the Δ^* resonance. This is not the case for the electromagnetic decay of Σ^* resonances. In principle, one can make use of the same procedure adopted for the K^* and N^* transition moment and take the ratio of the helicity amplitudes as a conversion coefficient. Due to the lack of knowledge about the latter quantities, we have used ratio's of the Σ ground state transition moments as conversion coefficients. This produces the following relations:

$$\kappa_{\Sigma^*\Sigma^0} = \frac{\mu_{\Sigma^0}}{\mu_{\Sigma^+}} \kappa_{\Sigma^*\Sigma^+} = \frac{\mu_{\Sigma^0}}{\mu_{\Sigma^-}} \kappa_{\Sigma^*\Sigma^-}, \quad \text{(A15)}$$

in which we have used $\mu_{\Sigma^+} = 2.458$, $\mu_{\Sigma^-} = -1.160$ [23], and $\mu_{\Sigma^0} = 0.79$ [24].

[1] M.Q. Tran *et al.*, Phys. Lett. B **445**, 20 (1998); http://lisa12.physik.uni-bonn.de/saphir/klks.txt
[2] S. Goers *et al.*, Phys. Lett. B **464**, 331 (1999); http://lisa12.physik.unibonn.de/saphir/web_values_k0si.txt
[3] W.-T. Chiang, F. Tabakin, T.-S. Lee, and B. Saghai, Phys. Lett. B **517**, 101 (2001).
[4] S. Janssen, J. Ryckebusch, D. Debruyne, and T. Van Cauteren, Phys. Rev. C **65**, 015201 (2002).
[5] T. Feuster and U. Mosel, Phys. Rev. C **59**, 460 (1999).
[6] M. Benmerrouche, N. Mukhopadhyay, and J. Zhang, Phys. Rev. D **51**, 3237 (1995).
[7] B. Pearce and B. Jennings, Nucl. Phys. **A528**, 655 (1991).
[8] R. Davidson and R. Workman, Phys. Rev. C **63**, 025210 (2001).
[9] K. Ohta, Phys. Rev. C **40**, 1335 (1989).
[10] H. Haberzettl, Phys. Rev. C **56**, 2041 (1997).
[11] T. Mart, C. Bennhold, and C. Hyde-Wright, Phys. Rev. C **51**, R1074 (1995).
[12] S. Capstick and W. Roberts, Phys. Rev. D **58**, 074011 (1998).
[13] Z. Li and F. Close, Phys. Rev. D **42**, 2207 (1990).
[14] P. Stassart and F. Stancu, Phys. Rev. D **42**, 1521 (1990).
[15] T. Mart and C. Bennhold, Phys. Rev. C **61**, 012201(R) (2000).

[16] T. Mart, Phys. Rev. C **62**, 038201 (2000).
[17] A.D. Martin, Nucl. Phys. **B179**, 33 (1981).
[18] A. Gasparian, J. Haidenbauer, C. Hanhart, L. Kondratyuk, and J. Speth, Nucl. Phys. **A684**, 397c (2001).
[19] B. Holzenkamp, K. Holinde, and J. Speth, Nucl. Phys. **A500**, 485 (1989).
[20] R. Williams, C.-R. Ji, and S. Cotanch, Phys. Rev. C **46**, 1617 (1992).
[21] M. Cheoun, B. Han, B. Yu, and I.-T. Cheon, Phys. Rev. C **54**, 1811 (1996).
[22] S. Hsiao, D. Lu, and S. Yang, Phys. Rev. C **61**, 068201 (2000).
[23] Particle Data Group, D.E. Groom *et al.*, Eur. Phys. J. C **15**, 1 (2000).
[24] D.H. Perkins, *Introduction to High Energy Physics*, 4th ed. (Cambridge University Press, Cambridge, 2000).
[25] S. Janssen, J. Ryckebusch, W. Van Nespen, D. Debruyne, and T. Van Cauteren, Eur. Phys. J. A **11**, 105 (2001).
[26] B. Saghai, nucl-th/0105001.
[27] F.X. Lee, T. Mart, C. Bennhold, H. Haberzettl, and L.E. Wright, Nucl. Phys. **A695**, 237 (2001).
[28] J. David, C. Fayard, G. Lamot, and B. Saghai, Phys. Rev. C **53**, 2613 (1996).
[29] C.-R. Ji and S. Cotanch, Phys. Rev. C **38**, 2691 (1988).
[30] H. Burkhardt, J. Lowe, and A. Rosenthal, Nucl. Phys. **A440**, 653 (1985).
[31] D.A. Whitehouse *et al.*, Phys. Rev. Lett. **63**, 1352 (1989).
[32] R. Workman and H. Fearing, Phys. Rev. D **37**, 3117 (1988).
[33] R. Schumacher, Nucl. Phys. **A663**, 440c (2000).
[34] A. D'Angelo, in *Proceedings of the NSTAR 2001 Workshop on The Physics of Excited Nucleons*, edited by D. Drechsel and L. Tiator (World Scientific, New Jersey, 2001), p. 347.
[35] R. Zegers, in *Proceedings of the International Symposium on Electromagnetic Interactions in Nuclear and Hadronic Physics*, edited by M. Fujiwara and T. Shima (World Scientific, New Jersey, 2001).
[36] K.-H. Glander, in *Proceedings of the NSTAR 2001 Workshop on The Physics of Excited Nucleons*, edited by D. Drechsel and L. Tiator (World Scientific, New Jersey, 2001), p. 381.
[37] T. Theussl, R. Wagenbrunn, B. Desplanques, and W. Plessas, Eur. Phys. J. A **12**, 91 (2001).
[38] P. Singer and G. Miller, Phys. Rev. D **33**, 141 (1986).